Journal of Power Sources 220 (2012) 449–454

Contents lists available at SciVerse ScienceDirect

Journal of Power Sources

journal homepage: www.elsevier.com/locate/jpowsour

Short communication

A robust fuel cell cathode catalyst assembled with nitrogen-doped carbon nanohorn and platinum nanoclusters

Linwei Zhang [a,b], Ning Zheng [a], Ang Gao [a], Chunmei Zhu [a], Zhiyong Wang [a], Yuan Wang [a,*], Zujin Shi [a,*], Yan Liu [a,*]

[a] Beijing National Laboratory for Molecular Sciences, State Key Lab for Structural Chemistry of Unstable and Stable Species, College of Chemistry and Molecular Engineering, Peking University, Beijing 100871, PR China
[b] College of Chemistry and Chemical Engineering, Lanzhou University, Lanzhou 730000, PR China

HIGHLIGHTS

- Pt/NSWCNH is assembled with Pt nanocluster and nitrogen-doped carbon nanohorns.
- Most of Pt nanoparticles are dispersed in the conductive nano-nets formed by NSWCNHs.
- Pt/NSWCNH shows higher durability and catalytic activity for ORR than commercial Pt/C.
- Pt in Pt/NSWCNH is more stable against particle size growth than that in Pt/C.

GRAPHICAL ABSTRACT

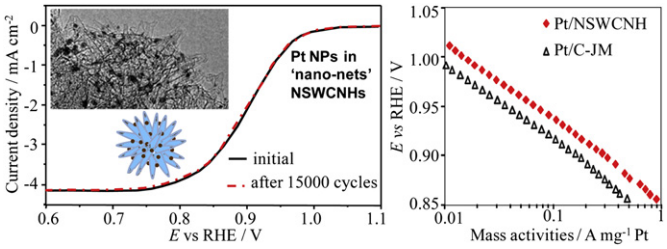

ARTICLE INFO

Article history:
Received 27 March 2012
Received in revised form
3 August 2012
Accepted 6 August 2012
Available online 11 August 2012

Keywords:
Catalytic cathode
Durability
Nitrogen-doped
Oxygen reduction reaction
Polymer electrolyte membrane fuel cells

ABSTRACT

A highly durable and active nanocomposite cathode catalyst (Pt/NSWCNH) is assembled with "unprotected" Pt nanoclusters and nitrogen-doped single-wall carbon nanohorns (NSWCNH) as building blocks by a convenient process. The specific catalytic activity and mass catalytic activity for the oxygen reduction reaction over Pt/NSWCNH is 1.60 and 1.75 times as high as those over a commercial Pt/C catalyst, respectively. There is no obvious loss in the catalytic activity of Pt/NSWCNH after potential cycling from 0.6 to 1.1 V versus RHE for 15,000 cycles at 30 °C, under the oxidizing conditions for the electrochemically catalytic reduction of O_2. TEM characterization results reveal that, during the accelerated aging tests, Pt nanoparticles in Pt/NSWCNH are more stable than that in Pt/C-JM, showing a low increase in the particle size.

1. Introduction

Cathode electrocatalysts with high stability and excellent catalytic activity for the oxygen reduction reaction (ORR) are a vital component of high-quality polymer electrolyte membrane fuel cells (PEMFCs) which provide electric power in a clean and convenient manner. Numerous efforts have been devoted to developing cathode catalysts of supported platinum-based nanoparticles (NPs) because the durability and catalytic activity of traditional Pt/C cathode catalysts are not high enough for real applications. Carbon supported Pt NPs modified with gold nanoclusters [1], $AuNi_{0.5}Fe$/Pt clusters with a core–shell structure [2], and Pt–Pd clusters with a particle-on-particle structure [3] showed

* Corresponding authors. Tel.: +86 10 62757497; fax: + 86 10 62765769.
E-mail addresses: wangy@pku.edu.cn (Y. Wang), zjshi@pku.edu.cn (Z. Shi), liu-yan@pku.edu.cn (Y. Liu).

0378-7753/$ – see front matter © 2012 Elsevier B.V. All rights reserved.
http://dx.doi.org/10.1016/j.jpowsour.2012.08.009

obviously enhanced durability for ORR compared to commercial Pt/C catalysts. Recently, Gupta and coworkers reported graphitic mesoporous carbon supported Pt–Cu bimetallic particles with a Pt shell, which exhibited excellent catalytic activity for ORR and high durability in a $HClO_4$ (0.1 mol L^{-1}) solution [4]. As demonstrated by the aforementioned progresses, Pt-based bimetallic or multi-metallic nanoparticles with some special nanostructures are promising building blocks for catalytic cathodes of PEMFCs. However, the metastable nanostructures of many active bimetallic or multi-metallic cathode catalysts are usually produced by complicated methods such as electrochemically etching or deposition processes, which will limits the application of such catalysts at a large scale. Moreover, it is well accepted that the recovery and purification of noble metals including Pt, Pd and Au from bimetallic or multi-metallic catalysts are much more complicated than that from monometallic catalysts. Therefore, the development of new supported monometallic Pt NPs catalysts with high durability and electrocatalytic activity for ORR is also of significance for promoting the utilization of PEMFCs.

The catalytic activity and stability of carbon supported metal catalysts are dependent on the structures and properties of the catalytic metals and support materials, as well as the interaction between them. With the development of carbon nanomaterials, more and more attention has been attracted to their application as catalyst supports [5–14]. Carbon nanotubes (CNTs) have been considered an attractive candidate for the support of PEMFCs catalysts owing to their high electric conductivity, stability, and specific surface area. However, the inert and smooth CNTs surfaces often caused difficulty in preparing electrocatalysts with a high metal loading and dispersion. Several surface modification processes have proven to be effective in improving the metal dispersion of metal/CNTs electrocatalysts [13–16]. It was reported that electrocatalysts prepared by supporting Pt NPs on surface–modified CNTs or functionalized graphene (FG) are more stable than that having a carbon black support (Pt/C) [15–18], but there are still great challenges in improving the activity and durability of these nanocomposite cathode catalysts.

Recently, some methods for synthesizing single-wall carbon nanohorns (SWCNHs) in a low cost manner have been developed [19,20]. SWCNHs supported Pt catalysts were prepared by the reduction of Pt oxide or hydroxide nanoparticles in the presence of SWCNH supports, and were reported to exhibit enhanced catalytic activity toward fuel cell reactions in comparison with Pt/C in PEMFCs [21–23]. However, to the best of our knowledge, there is not any report about the stability of the previously reported SWCNHs supported Pt catalysts.

Herein we report a novel nanocomposite cathode catalyst (Pt/NSWCNH) which was assembled using “unprotected” Pt nanoclusters [24] with an average diameter of 1.7 nm and nitrogen-doped single-wall carbon nanohorns (NSWCNHs) as building blocks. The self-assembly of Pt/NSWCNH was characterized by inserting most of the Pt nanoparticles in nano-networks formed by stacking of NSWCNHs. The present Pt/NSWCNH catalyst exhibited higher catalytic activity for ORR and strikingly enhanced stability compared to a commercial Pt/C catalyst (Pt/C-JM, which was used as a reference in many publications).

2. Experimental

2.1. Materials

A carbon supported Pt catalyst (Pt/C-JM, Pt: 9.4 wt. %) was purchased from Johnson Matthey Company. Carbon black (Vulcan XC-72R, BET = 256 m^2 g^{-1}) and a Nafion® solution (5 wt. %) were purchased from Cabot Corporation and Aldrich, respectively. $H_2PtCl_6 \cdot 6H_2O$ (AR grade) was supplied by Sinopharm Chemical Reagent Beijing co. ltd., perchloric acid, sodium hydroxide, ethylene glycol and ethanol (AR grade) were purchased from Beijing Chemical Corp.

2.2. Catalyst synthesis

NSWCNHs containing 1.6 wt. % of N applied in this work were prepared by a DC arc discharge method in air, and was heated at 400 °C in air for 4 h to remove amorphous carbon [20]. “Unprotected” Pt nanoclusters (stabilized with ethylene glycol and simple ions) with an average diameter of 1.7 nm used in this work were prepared according to the previously reported methods [24]. In a typical synthesis of Pt/NSWCNH, 45 mg of NSWCNHs powder was dispersed ultrasonically in a C_2H_5OH/H_2O mixture (40 mL, volume ratio = 1:1) for 30 min. Then a prepared colloidal solution of Pt nanoclusters (1.35 mL, Pt: 3.7 g L^{-1}) was added dropwise to the suspension under stirring, followed by ultrasonically treating the mixture for 20 min. After stirring overnight, solid in the suspension was filtered, leaving a colorless solution, washed with ultra–pure water (18 MΩ) and C_2H_5OH, dried at 40 °C, and then heated at 300 °C in a tube furnace under nitrogen for 1 h to obtain Pt/NSWCNH as a black powder. A homemade Pt/C powder (Pt/C-HM) was prepared by the same method using a carbon black support (Vulcan XC-72R) and the same colloidal solution of Pt nanoclusters as starting materials.

2.3. Rotating disk electrode measurements

Rotating disk electrode (RDE) measurements were performed in a conventional three-compartment electrochemical cell containing an aqueous solution of $HClO_4$ (0.1 mol L^{-1}), in which a Ag/AgCl electrode was used as the reference electrode and a platinum foil was used as the counter electrode. All potentials in this work were referred to a relative hydrogen electrode (RHE) scale. The working electrodes were prepared as follows: Pt/NSWCNH or Pt/C catalysts (10 mg), a Nafion® solution (100 μL, 5 wt.%) and C_2H_5OH (5 mL) were mixed ultrasonically for 20 min. 20 μL of the obtained suspension was transferred onto a freshly polished glassy carbon disk electrode (0.196 cm^2) and dried at room temperature.

Cyclic voltammetry (CV) was conducted between 0.05 and 1.2 V at 50 mV s^{-1} in N_2-saturated $HClO_4$ solutions, and the specific electrochemical surface area of Pt particles (SESA, m^2 g^{-1}Pt) was calculated from cyclic voltammograms by integrating the area in the hydrogen underpotential deposition (H_{UPD}) region using Eq. (1):

$$\mathrm{SESA} = \frac{100 Q_H}{210 \cdot L_{Pt} \cdot A} \qquad Q_H = \frac{Q_{Hads} + Q_{Hdes}}{2} \tag{1}$$

where Q_{Hads} and Q_{Hdes} (μC) are the charges associated with the hydrogen adsorption and desorption, respectively. L_{Pt} is the Pt loading (μg cm^{-2}), A is the geometric area of the glassy carbon (cm^2), and the value of 210 μC cm^{-2} is an average charge density associated with the formation of one monolayer hydrogen atoms on a polycrystalline platinum surface [25].

Oxygen reduction activities were measured at 1600 rpm and 30 °C in an aqueous solution of $HClO_4$ (0.1 mol L^{-1}) by positive-going potential sweeps from 0.05 to 1.2 V versus RHE at a scan rate of 10 mV s^{-1}. ORR polarization curves were obtained from the difference of current densities between O_2 and N_2 atmosphere, ($i_{O2\text{-}N2} = i_{O2}\text{-}i_{N2}$).

2.4. Accelerated aging tests for catalysts

The working electrodes used in accelerated aging tests (AAT) were heated at 120 °C in a vacuum oven for 1 h after dried at room temperature. Potential scans were carried out between 0.6 and 1.1 V at 30 and 60 °C in an O_2-saturated aqueous solution of $HClO_4$ (0.1 mol L^{-1}) under stirring. The electrochemical catalytic activities of the electrodes before and after AAT were evaluated by positive-going potential sweeps from 0.05 to 1.20 V versus RHE at a scan rate of 5 mV s^{-1}. The electrochemical surface areas of Pt before and after AAT were measured as aforementioned.

2.5. Characterizations and instruments

The morphologies of catalysts were studied by transmission electron microscope (TEM, FEI Tecnai G^2F20). X-ray diffraction measurements were carried out on a Rigaku-2500Pc X-ray diffractometer with Cu radiation at 40 kV and 300 mA. Inductively coupled plasma atomic emission spectrometry (ICP-AES, Leeman Co.) was used to analyze the content of Pt in the prepared Pt/NSWCNH and Pt/C catalysts. The content of N in the prepared NSWCNH and Pt/NSWCNH powders was analyzed by elementary analysis (Elementar vario MICRO CUBE, vario EL, Elementar Analysensysteme, Germany). XPS measurements were carried out with an Axis Ultra photoelectron spectrometer with a monochromatic Al$K\alpha$ X-ray (1486.7 eV) source. The binding energies were referenced to the C 1s binding energy of contamination carbon at 284.5 eV. Electrochemical tests of the prepared electrodes were conducted using Model CHI 660C workstation. The current densities were expressed in terms of the geometric surface area of the electrodes except where otherwise indicated.

3. Results and discussion

3.1. Characterizations of the catalysts

Fig. 1 shows the TEM images and the size distributions of Pt nanoparticles in Pt/NSWCNH (a–b), Pt/C-JM (c–d) and Pt/C-HM (e–f). The size distributions of Pt particles in the catalyst were obtained based on the measurements of 300 Pt particles in the sample. The uncertainty of the measurements is 0.2 nm. As shown in Fig. 1a, NSWCNH knitted to form electroconductive nano-nets in Pt/NSWCNH and most of the Pt nanoparticles were well dispersed in the nano-nets. Some Pt nanoparticles were also observed inside the NSWCNH (as marked by the arrow in the insert). The Pt nanoparticles in the prepared Pt/NSWCNH and Pt/C-HM catalysts have the same average diameter (d_{av}) of 1.9 nm as measured by TEM (Fig. 1b and f), which is smaller by 14% than that of Pt particles in the Pt/C-JM catalyst ($d_{av} = 2.2$ nm, Fig. 1d). The Pt contents of Pt/NSWCNH and Pt/C-HM were 9.1 and 9.2 wt. %, respectively, as measured by ICP-AES. Elementary analysis showed that Pt/NSWCNH contained 1 wt.% of N. Fig. 2 shows the N 1s region of X-ray photoelectron spectroscopy from Pt/NSWCNH. Nitrogen atoms in NSWCNHs might mainly exist in the form of pyridinic-type N [26] as indicated by the N 1s binding energy value of 399.0 eV measured in this work, although N 1s signals with higher binding energies were also observed.

Fig. 3 shows the X-ray diffraction (XRD) patterns of the NSWCNHs, Pt/NSWCNH and Pt/C-JM powders, in which the diffraction peaks related to the (002) and (100) planes of the hexagonal graphite structure appear at positions near 26 and 42°, respectively. A broad peak centered at 25° in the diffraction pattern of Pt/C-JM is the signal from carbon black which is characterized by small regions of ordered structures. The diffraction patterns of NSWCNHs and Pt/NSWCNH samples show two sharp peaks at 25.8°

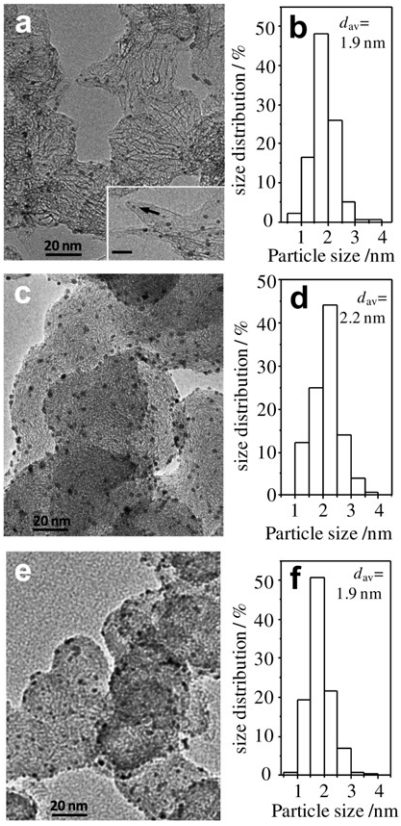

Fig. 1. TEM images and the size distributions of Pt nanoparticles in Pt/NSWCNH (a–b), Pt/C-JM (c–d) and Pt/C-HM (e–f). The bar expresses 10 nm in the insert of (a).

and 26.4°. The stronger one at 26.4° could be attributed to the signal from a small amount of graphite present in the sample, while the peak at 25.8° could be ascribed to the signal from NSWCNHs. The XRD patterns of SWCNHs synthesized by a laser vaporization method showed a broad shoulder peak centered at 22° (close to the diffraction signal of graphite (002) planes), which was intensively investigated by Iijima and coworkers and was explained by a double layer diffraction model associated with two graphene sheets in their SWCNH aggregates [21]. The corresponding diffraction signal as a weak shoulder peak centered at 25° of SWCNHs synthesized by an AC arc discharge method was observed

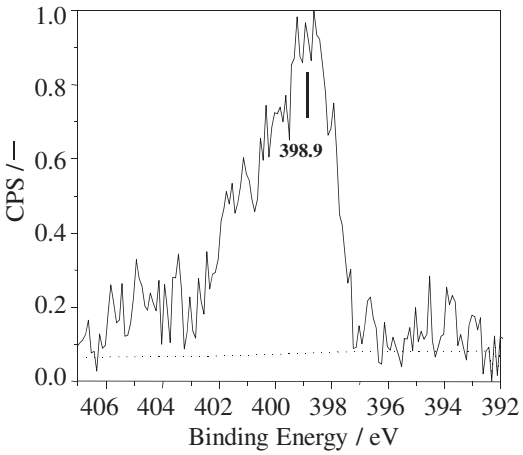

Fig. 2. N 1s X-ray photoelectron spectroscopy of Pt/NSWCNH.

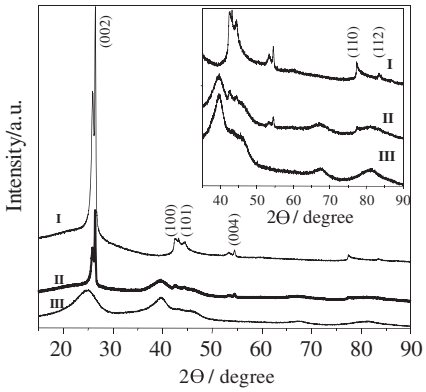

Fig. 3. X-ray diffraction patterns of the NSWCNH (I), Pt/NSWCNH (II) and Pt/C-JM (III) catalysts.

later [27]. The difference in shape of the diffraction peaks relating to the stacked nanohorns between the reported SWCNH and our NSWCNH samples may reflect the different stacking manner of the nanohorns or the different order degrees of the walls. Typical peaks at 39.8°, 67.5° and 81.3° assignable to the signals from the (111), (220) and (311) planes of fcc Pt, respectively, can be observed in the XRD patterns of Pt/NSWCNH and Pt/C-JM.

3.2. Electrocatalytic activity for ORR

Fig. 4 shows the electrochemical properties of NSWCNH, Pt/NSWCNH, Pt/C-HM and Pt/C-JM. The specific electrochemical surface areas of Pt (SESA) in Pt/NSWCNH, Pt/C-HM and Pt/C-JM electrodes were calculated to be 83, 82 and 74 $m^2\ g^{-1}$. As shown in Fig. 4b, no reduction current for ORR was observed above 0.4 V over NSWCNH, while Pt/NSWCNH exhibited a more positive on-set potential, indicating that Pt/NSWCNH is more active than Pt/C-JM and Pt/C-HM for catalyzing ORR. The specific kinetic current density (i_k) is independent of diffusion and is widely used to evaluate the intrinsic catalytic activity of electrocatalysts [1,2,28]. i_k was calculated from the experimental data using the Koutecky-Levich equation:

$$i_k = \frac{i \cdot i_d}{i_d - i} \tag{2}$$

where i is the experimentally obtained current, i_d refers to the measured diffusion–limited current, and i_k is the mass transport free kinetic current. The specific catalytic activities and mass catalytic activity can be determined via calculation of i_k using Eq. (2) and normalization with the Pt surface area and the Pt loading, respectively. The specific catalytic activity over Pt/NSWCNH at 0.9 V (0.367 mA cm^{-2} Pt) was 1.60 times as high as that over Pt/C-JM (0.235 mA cm^{-2} Pt, Fig. 4c), indicating an obvious enhancement in the intrinsic catalytic activity for ORR. As shown in Fig. 4d, the mass catalytic activity over Pt/NSWCNH (0.305 A mg^{-1}Pt) was larger by 75% than that over Pt/C-JM (0.174 A mg^{-1}Pt). The catalytic activity over Pt/C-HM was close to that of Pt/C-JM. It should be mentioned that the specific activity is an important parameter for investigating the properties of catalytic sites in catalysts, however, the mass activity is the valuable one for real application. The mass catalytic activity (0.305 A mg^{-1}Pt) at 0.9 V vs. RHE of Pt/NSWCNH catalyst was undoubtedly superior to not only that of commercially available Pt/C catalysts, but also that of most previously reported Pt/C catalysts (ca. 0.16 [29]–0.24 [30] A mg^{-1}Pt) with various structures.

Since NSWCNH is inactive for catalyzing ORR at 0.9 V, and the catalytic activity over Pt/C-HM having the similar Pt particles as Pt/NSWCNH is close to that over Pt/C-JM, we believe that the interaction between NSWCNH and the Pt particles are responsible for the enhanced catalytic activity [31]. As indicated by Radovic et al. [32], an enhanced Lewis basicity derived from strong π electron delocalization of N-doped carbons could increase the electron-

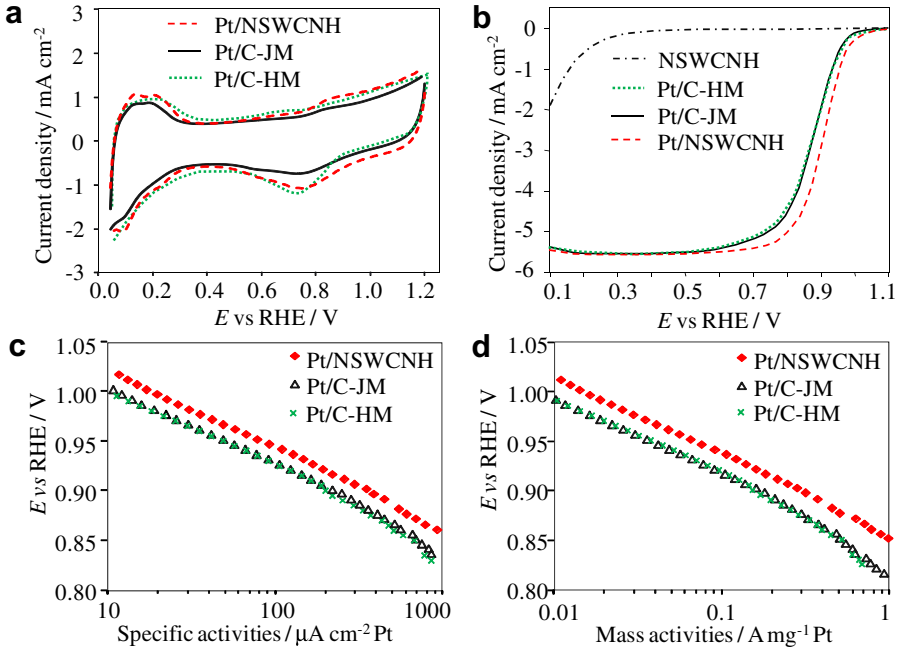

Fig. 4. Electrochemical properties of the Pt/NSWCNH (16.7 μgPt cm^{-2}), Pt/C-HM (17.2 μgPt cm^{-2}), and Pt/C-JM (17.4 μgPt cm^{-2}) electrodes tested in $HClO_4$ (0.1 mol L^{-1}) aqueous solution at 30 °C. (a) CV at a scan rate of 50 mV s^{-1} under N_2, (b) ORR polarization curves at 1600 rpm with a scan rate of 10 mV s^{-1}, (c) specific catalytic activities, and (d) mass catalytic activities. The measurement error is 3%.

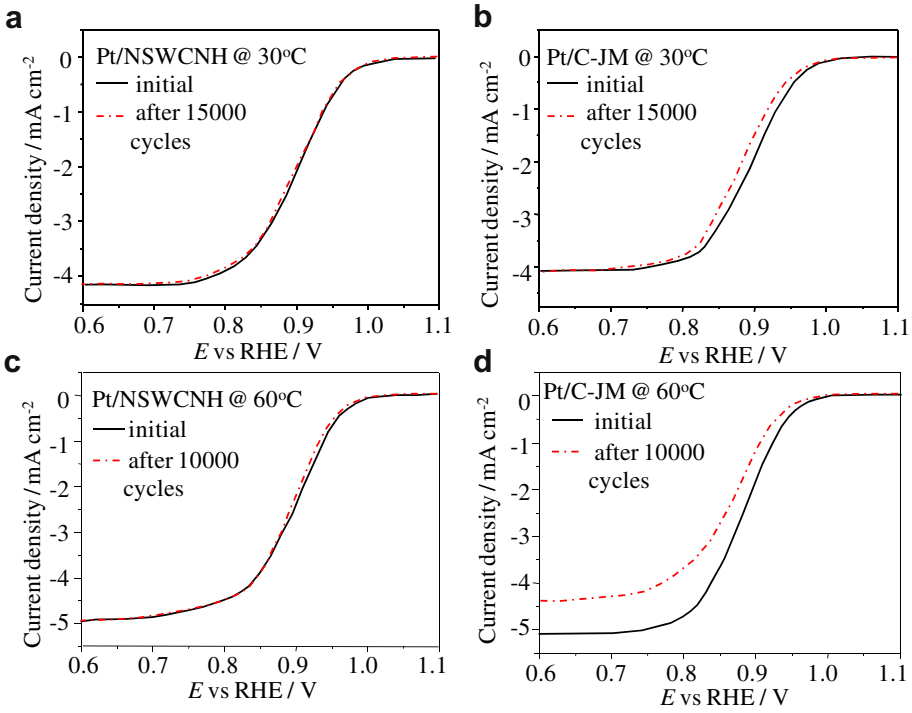

Fig. 5. ORR polarization curves (5 mV s^{-1}) of Pt/NSWCNH (a, c) and Pt/C-JM (b, d) tested before and after potential cycling from 0.6 to 1.1 V in an O_2-saturated $HClO_4$ solution at 30 and 60 °C.

donor capacity of carbon, which might be a cause of the enhanced catalytic activity for ORR [31].

3.3. Electrochemical stability

The electrochemical stability of the Pt/NSWCNH and Pt/C-JM electrodes was evaluated by accelerated aging tests (AAT) at 30 and 60 °C, i.e. by cycling the potential between 0.6 and 1.1 V in an O_2-saturated $HClO_4$ solution (0.1 mol L^{-1}). Fig. 5 shows ORR polarization curves of the Pt/NSWCNH and Pt/C-JM electrodes before and after AAT at 30 and 60 °C, respectively. For the Pt/NSWCNH electrode (Fig. 5a), the polarization curves almost overlap, suggesting no obvious loss in the catalytic activity and the half-wave potential ($E_{1/2}$) after the aforementioned potential cycling test ($E_{1/2}(I) = 0.904$ V, $E_{1/2}(F) = 0.902$ V, where I and F denote before and after 15,000 potential cycles, respectively). Whereas for the Pt/C-JM electrode, a decrease by 17% in the catalytic activity at 0.9 V, and a decrease by 18 mV in the half-wave potential were observed after the same potential cycling test. Moreover, ESA of Pt/NSWCNH decreased by ca. 6%, while that of Pt/C-JM decreased by 43% after the aforementioned tests (Table 1). AAT at 60 °C showed the enhanced durability of Pt/NSWCNH relative to Pt/C-JM more clearly. The catalytic activity at 0.9 V decreased by 10 and 33% over Pt/NSWCNH and Pt/C-JM, respectively.

TEM images and the size distributions of Pt NPs in the catalysts used in AAT at 60 °C were measured to understand the enhanced durability of Pt/NSWCNH (Fig. 6). Obvious increase in the particle size of Pt NPs in the used Pt/C-JM catalyst occurred, with increasing d_{av} from 2.2 to 3.3 nm, while the size increase extent of Pt NPs in Pt/NSWCNH was much less than that in Pt/C-JM during the AAT tests, with a growth in d_{av} from 1.9 to 2.3 nm. From the size distributions

Table 1
Catalytic activity and electrochemical surface area of Pt/NSWCNH and Pt/C-JM before and after AAT.[a]

Catalytic cathode	T °C	before AAT		After AAT	
		j/mA cm^{-2}	ESA/cm^2	j/mA cm^{-2}	ESA/cm^2
Pt/NSWCNH	30	2.15	3.2	2.09	3.0
Pt/C-JM	30	1.78	3.0	1.47	1.7
Pt/NSWCNH	60	2.44	3.1	2.20	2.2
Pt/C-JM	60	1.97	2.8	1.32	1.5

[a] AAT conditions: cycling the potential between 0.6 and 1.1 V in an O_2-saturated aqueous solution of $HClO_4$ (0.1 mol L^{-1}) at 30 and 60 °C for 15,000 and 10,000 cycles, respectively. The current density at 0.9 V was used to evaluate the catalytic activities. The measurement error is 3%.

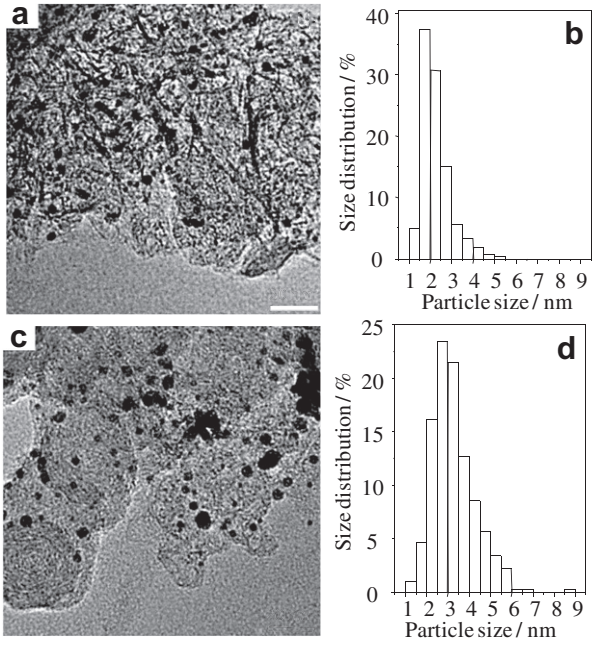

Fig. 6. TEM images and the size distribution of Pt nanoparticles in the Pt/NSWCNH (a–b) and Pt/C-JM (c–d) electrodes after AAT at 60 °C.

shown in Fig. 6, it can be seen that the percentage of Pt NPs with diameters less than 3 nm in used Pt/NSWCNH was 88%, while that in used Pt/C-JM was only 45%. Therefore, the degradation in ESA and catalytic activity of Pt/C-JM should mainly derived from the increase of Pt nanoparticle size, although the dissolution of Pt metals into the electrolyte and the detachment of Pt nanoparticles from the corroded carbon support might also contribute to the degradation.

According to the aforementioned results, we believe that the excellent stability of Pt/NSWCNH are mainly derived from trapping the Pt nanoparticles in the NSWCNH nano-network, suppressing the migration, aggregation, and growth in size of small Pt nanoclusters during the potential cycles. Moreover, the high graphitization degree or ordered structure of the NSWCNH walls will weaken the support degradation caused by Pt–catalyzed oxidation of carbon supports, which may be another cause of the enhanced durability relative to that of Pt/C-JM. The influence of electronic interactions between the Pt nanoclusters and NSWCNH on the catalytic activity and durability is still an open question.

4. Conclusions

In conclusion, the Pt/NSWCNH catalyst assembled with "unprotected" Pt colloidal nanoparticles and nitrogen-doped single-wall carbon nanohorns as building blocks exhibited obviously enhanced durability and catalytic activity for ORR compared to commercially available Pt/C catalysts. At 0.9 V versus RHE, the mass catalytic activity and specific catalytic activity for ORR over Pt/NSWCNH are 75% and 60% larger than those over Pt/C-JM, respectively. No obvious loss in the catalytic activity of the present Pt/NSWCNH catalyst was detected after 15,000 potential cycles between 0.6 and 1.1 V at 30 °C in an aqueous solution of $HClO_4$ (0.1 mol L^{-1}). Whereas the decrease in the catalytic activity over Pt/C-JM was 17% after the same potential cycling test. The enhanced durability of Pt/NSWCNH relative to Pt/C-JM was further confirmed by accelerated aging tests at 60 °C, in which, after 10,000 potential cycles between 0.6 and 1.1 V, the catalytic activity at 0.9 V over Pt/NSWCNH and Pt/C-JM decreased by 10 and 33%, respectively. TEM characterization results revealed that during the accelerated aging tests, Pt NPs in Pt/NSWCNH is more stable against growth in the particle size than that in Pt/C-JM, which is an important cause of the obviously enhanced durability of Pt/NSWCNH. In view of its outstanding electrochemical stability, excellent catalytic activity for ORR, simple composition and convenient preparation process, Pt/NSWCNH is a promising cathode catalyst for fuel cells.

Acknowledgments

This work is jointly supported by NSFC (grants 20803001, 20973003, 51121091, 21171013, 21133001), and Chinese Ministry of Science and Technology (NKBRSF 2011CB 808702 and 2011CB 932601).

References

[1] J. Zhang, K. Sasaki, E. Sutter, R.R. Adzic, Science 315 (2007) 220–222.
[2] K. Gong, D. Su, R.R. Adzic, J. Am. Chem. Soc. 132 (2010) 14364–14366.
[3] Z.M. Peng, H. Yang, J. Am. Chem. Soc. 131 (2009) 7542–7543.
[4] G. Gupta, D.A. Slanac, P. Kumar, J.D. Wiggins-Camacho, X. Wang, S. Swinnea, K.L. More, S. Dai, K.J. Stevenson, K.P. Johnston, Chem. Mater. 21 (2009) 4515–4526.
[5] S. Iijima, Nature 354 (1991) 56–58.
[6] T.W. Ebbesen, P.M. Ajayan, Nature 358 (1992) 220–222.
[7] A. Thess, R. Lee, P. Nikolaev, H. Dai, P. Petit, J. Robert, C. Xu, Y.H. Lee, S.G. Kim, A.G. Rinzler, D.T. Colbert, G.E. Scuseria, D. Toma′ nek, J.E. Fischer, R.E. Smalley, Science 273 (1996) 483–487.
[8] S.H. Joo, S.j. Choi, I. Oh, J. Kwak, Z. Liu, O. Terasaki, R. Ryoo, Nature 412 (2001) 169–172.
[9] T. Hyeon, S. Han, Y.-E. Sung, K.-W. Park, Y.-W. Kim, Angew. Chem. Int. Ed. 42 (2003) 4352–4356.
[10] T. Maiyalagan, B. Viswanathan, U.V. Varadaraju, Electrochem. Commun. 7 (2005) 905–912.
[11] Z.H. Wen, J. Liu, J.H. Li, Adv. Mater. 20 (2008) 745.
[12] K.P. Gong, F. Du, Z.H. Xia, M. Durstock, L.M. Dai, Science 323 (2009) 760–764.
[13] W.Z. Li, C.H. Liang, W.J. Zhou, J.S. Qiu, Z.H. Zhou, G.Q. Sun, Q. Xin, J. Phys. Chem. B 107 (2003) 6292–6299.
[14] S.F. Zheng, J.S. Hu, L.S. Zhong, L.J. Wan, W.G. Song, J. Phys. Chem. C 111 (2007) 11174–11179.
[15] Y. Shao, G.P. Yin, Y.Z. Gao, P.F. Shi, J. Electrochem. Soc. 153 (2006) A1093–A1097.
[16] R. Kou, Y. Shao, D. Wang, M.H. Engelhard, J.H. Kwak, J. Wang, V.V. Viswanathan, C. Wang, Y. Lin, Y. Wang, I.A. Aksay, J. Liu, Electrochem. Commun. 11 (2009) 954–957.
[17] Y.G. Chen, J.J. Wang, H. Liu, M.N. Banis, R.Y. Li, X.L. Sun, T.K. Sham, S.Y. Ye, S. Knights, J. Phys. Chem. C 115 (2011) 3769–3776.
[18] Frédéric Hasché, M. Oezaslana, P. Strasser, Phys. Chem. Chem. Phy. 12 (2010) 15251–15258.
[19] N. Sano, J. Phys. D Appl. Phys. 37 (2004) L17–L20.
[20] N. Li, Z.Y. Wang, K.K. Zhao, Z.J. Shi, Z.N. Gu, S.K. Xu, Carbon 48 (2010) 1580–1585.
[21] T. Yoshitake, Y. Shimakawa, S. Kuroshima, H. Kimura, T. Ichihashi, Y. Kubo, D. Kasuya, K. Takahashi, F. Kokai, M. Yudasaka, S. Iijima, Phys. B Condens. Matter 323 (2002) 124–126.
[22] M. Kosaka, S. Kuroshima, K. Kobayashi, S. Sekino, T. Ichihashi, S. Nakamura, T. Yoshitake, Y.J. Kubo, J. Phys. Chem. C 113 (2009) 8660–8667.
[23] S. Bandow, F. Kokai, K. Takahashi, M. Yudasaka, L. C.Qin, S. Iijima, Chem. Phys. Lett. 321 (2000) 514–519.
[24] Y. Wang, J.W. Ren, K. Deng, L.L. Gui, Y.Q. Tang, Chem. Mater. 12 (2000) 1622–1625.
[25] A. S-Sheppard, S.A. Campbell, J.R. Smith, G.W. Lloyd, T.R. Ralph, F.C. Walsh, Analyst 123 (1998) 1923–1929.
[26] S. Pylypenko, A. Queen, T.S. Olson, A. Dameron, K. O'Neill, K.C. Neyerlin, B. Pivovar, H.N. Dinh, D.S. Ginley, T. Gennett, R. O'Hayre, J. Phys. Chem. C 115 (2011) 13667–13675.
[27] L. Brandão, C. Passeira, D.M. Gattia, A.J. Mendes, J. Mater. Sci. 46 (2011) 7198–7205.
[28] (a) A.J. Bard, L.R. Faulkner, Electrochemical Methods–Fundamentals and Application, second ed., John Wiley & Sons, New York, 2001;
(b) W. Vielstich, A. Lamm, H.A. Gasteiger, Handbook of Fuel Cells, Fundamentals Technology and Applications, vol. 2, John Wiley & Sons Ltd, 2003.
[29] X. Li, S. Park, B.N. Popov, J. Power Sources 195 (2010) 445–452.
[30] R. Balgisa, G.M. Anilkumarb, S. Sago, T. Ogia, K. Okuyama, J. Power Sources 203 (2012) 26–33.
[31] Y. Liu, N. Zheng, W. Chao, H.Q. Liu, Y. Wang, Electrochim. Acta 55 (2010) 5617–5623.
[32] C.A.L.Y. Leon, J.M. Solar, V. Calemma, L.R. Radovic, Carbon 30 (1992) 797–811.